Dalton Transactions

PAPER

View Article Online
View Journal | View Issue

Check for updates

Cite this: *Dalton Trans.*, 2019, **48**, 12440

Received 18th June 2019,
Accepted 19th July 2019

DOI: 10.1039/c9dt02567g

rsc.li/dalton

Microwave assisted synthesis of heterometallic 3d–4f M_4Ln complexes†

L. Rosado Piquer, [a,b] S. Dey,[c] L. Castilla-Amorós,[a] S. J. Teat, [d] J. Cirera, [a,e] G. Rajaraman [c] and E. C. Sañudo *[a,b]

In this paper we describe the synthesis and magnetic properties of a series of 3d–4f complexes of general formula $[M_4Ln(OH)_2(chp)_4(SALOH)_5(H_2O)(MeCN)(Solv)]$ (Solv = MeOH, MeCN, H_2O; chp stands for deprotonated 6-chloro-2-hydroxypyridine (C_5H_3ClNO), SALOH stands for monodeprotonated 3,5-ditert-butylsalicylic acid ($C_{15}H_{21}O_3$)) obtained by a solvent-free microwave assisted synthesis method. The Ni(II) complexes (**Ni_4Gd**, Solv = MeOH; **Ni_4Dy**, Solv = MeCN) are not SMMs in the absence of an applied dc field. The replacement of Ni(II) by Co(II) (**Co_4La**, Solv = MeOH; **Co_4Gd**, Solv = H_2O; **Co_4Gd**-MeCN, Solv = MeCN; **Co_4Tb**, Solv = MeOH; **Co_4Dy**, Solv = H_2O) results in improved SMM properties.

Introduction

Interest in molecular nanomagnets due to their potential applications in high-density information storage, molecular spintronics, quantum computing[1–3] or magnetic coolers[4] has grown in the last 30 years. Since the discovery of the first single-molecule magnet (SMM) $Mn_{12}Ac$ in the 90's by Christou[5] and Gatteschi,[6] the synthesis of high nuclearity complexes with SMM properties is a great and challenging target for coordination chemists. An SMM must have a large spin ground state and easy axis anisotropy, leading to slow relaxation of the magnetization below its blocking temperature. Thus, an SMM is able to retain the magnetization and it behaves like a magnet at the molecular level.[7,8] SMMs were also obtained using other 3d transition metals including manganese, iron, nickel, cobalt or vanadium,[9] but in these cases higher working temperatures have been elusive. Thus, the anisotropy barrier for the reversal of the magnetization in transition metal SMMs depends on two properties: the total spin of the molecule S and the Ising-type anisotropy. This knowledge has been used to design improved SMMs based on two strategies: rising S or increasing the anisotropy of the molecule. Increasing S by introducing stronger ferromagnetic coupling has been achieved in several examples: Mn_{18},[10] Mn_{21},[11] Mn_{84}[12] or Mn_{19}.[13] However, higher nuclearity structures with a large *S* value is no guarantee of a large molecular anisotropy. A great example is Mn_{19}: it possesses the record spin of 83/2 for a molecular cluster, but it lacks anisotropy and thus it is not an SMM. Focus is set since the early 2000s in increasing the magnetic anisotropy of the prepared complexes in order to improve SMM properties, using metal ions with strong spin–orbit coupling as Co(II) or the lanthanides. Heterometallic 3d–4f compounds as well as pure 4f systems are seen as the route to better SMMs. Rare earths have long been used in magnetism due to their strong magnetic anisotropy. 4f complexes usually have high energy barriers compared with 3d metals SMMs but their hysteresis loops are usually closed due to fast QTM (Quantum Tunnelling of the Magnetization) and alternative relaxation pathways.[14,15] Since the first heterometallic 3d–4f SMM was reported in 2004, many groups have devoted much effort to these 3d–4f complexes.[16] Still, in 2018 high operational temperatures for 4f or 3d–4f SMMs remain elusive. In 2018, after his previous work on organometallic lanthanide SMMs,[17–19] Layfield reported a nearly linear Dy metallocenium that displayed hysteresis at 80 K.[20] Reta and Chilton offered theoretical insight on the high temperature hysteresis, relating it once again to the coupling with vibrational phonons in the structure.[21] The last results greatly improved the archetypical lanthanide SMMs, the phthalocyanine lanthanide sandwich complexes first studied as SMMs by Ishikawa *et al.*[22–24]

The synthetic methodologies are crucial for obtaining homo- or heteronuclear complexes with the desired properties,

[a]*Departament de Química Inorgànica i Orgànica, Secció Química Inorgànica, Universitat de Barcelona, C/Martí i Franqués 1-11, 08028 Barcelona, Spain. E-mail: esanudo@ub.edu*
[b]*Institut de Nanociència i Nanotecnologia, Universitat de Barcelona, C/Martí i Franqués 1-11, 08028 Barcelona, Spain*
[c]*Department of Chemistry, Indian Institute of Technology Bombay, Powai, Mumbai, 400076, India*
[d]*Advanced Light Source, Lawrence Berkeley National Laboratory, Berkeley, CA 94720, USA*
[e]*Institut de Química Teòrica i Computacional, Universitat de Barcelona, C/Martí i Franqués 1-11, 08028 Barcelona, Spain*

†Electronic supplementary information (ESI) available. CCDC 1915070, 1878755, 1835341, 1878760 and 1878756. For ESI and crystallographic data in CIF or other electronic format see DOI: 10.1039/c9dt02567g

but most are still based on serendipitous assembly.[25] The interest on finding new synthetic methodologies is a challenge in chemistry.[26] In the last few years, microwave assisted synthesis has been useful for organic chemists not only to synthesize products that are otherwise unattainable, also to obtain in pure form products that in conventional conditions appear in a mixture that requires taxing purification methods. In the same way, this synthetic method is useful for the synthesis of high nuclearity coordination compounds.[27] In general, with microwave assisted synthesis, formation of one species is favoured.[28] Microwave assisted synthesis is clean, quick and it is included in green chemistry, because of its partial or in some cases total absence of organic solvents.[29] The microwave reactor offers a unique environment, which allows high temperatures and high pressure, generated by the heating of the molecules by the microwave radiation. Microwave energy is delivered directly to materials through molecular interaction with the electromagnetic field.[30] Only those substances with a dipolar moment will be excited by microwaves. This energy transfer to some of the species in the reaction mixture is very efficient and the heating rate is homogeneous.[31] The technique has been used to synthesize polynuclear coordination compounds like Ni_8 and Ni_9 [32] or Mn_3,[33] MOF's (Metal–Organic Frameworks)[34] and nanoparticles.[35] Solvent-free synthetic methods are often used in coordination chemistry, in a melt state[36–40] or by sublimation of the product.[41] Of particular relevance to spintronics is the archetypical mononuclear single molecule magnet (SMM) $TbPc_2$,[22] synthesized by conventional heating over long periods of time and that often produce mixtures of products and require tedious purification methods.[42,43]

In 2017 we used solvent-free microwave assisted synthesis to obtain $[Ni_4Tb(OH)_2(chp)_4(SALOH)_5(H_2O)(MeCN)(MeOH)]$ (**Ni_4Tb**) and its La analogue, **Ni_4La**.[44] Clearly, the prepared complexes were very interesting to us and we wanted to extend the synthetic method to other lanthanide ions and other transition metals. We herein exploit this synthetic method to prepare a family of M_4Ln complexes of general formula $[M_4Ln(OH)_2(chp)_4(SALOH)_5(H_2O)(MeCN)(Solv)]$ (Solv = MeOH, MeCN, H_2O) (**Ni_4Gd**, Solv = MeOH; **Ni_4Tb**-b, Solv = MeOH; **Ni_4Dy**, Solv = MeCN; **Co_4La**, Solv = MeOH; **Co_4Gd**, Solv = H_2O; **Co_4Gd**-MeCN, Solv = MeCN; **Co_4Tb**, Solv = MeOH; **Co_4Dy**, Solv = H_2O) and its by-products. The change of Ni(II) for Co(II) leads to an improvement on the SMM properties of the prepared complexes, as the cobalt complexes display SMM properties in the absence of an applied dc field.

Results and discussion

Following our work on microwave assisted synthesis in coordination chemistry we decided to apply the method to solvent-free systems. This would provide a clean, cost and time efficient method to obtain heterometallic coordination complexes. The clear limitation of the method is only that the ligands chosen must have easily attainable melting points in order to provide a good molten media for ion diffusion.

Microwave assisted synthesis was used to obtain new 3d–4f molecular nanomagnets with two versatile ligands (2-hydroxy-6-chloropyridine, Hchp, melting point 128–130 °C and 3,5-ditertbutylsalycilic acid, $SALOH_2$, (melting point 157–162 °C)) chosen due to their many possible coordination modes and their low melting points. The *tert*-butyl groups also improve solubility, processability of SMMs and self-organization on a metal surface.[45–47] The metal salts used are the metal hydroxides, freshly prepared, since they provide useful OH-counterions that are desired bridges in the final products. In 2017 we reported complex **Ni_4Tb** $[Ni_4Tb(OH)_2(chp)_4(SALOH)_5(H_2O)(MeCN)(MeOH)]$ and its La analogue.[44] Homometallic reactions in a similar ligand system have been reported elsewhere.[48]

Following this work on homometallic and heterometallic reactions with a versatile ligand system we decided to extend this chemistry to other transition metals and to study the reaction system in different reaction conditions. Three different reaction methods were studied: (a) solvent-free microwave assisted synthesis, (b) microwave assisted synthesis in solvent and (c) bench-top stirring reactions at room temperature.

The solvent free microwave assisted reaction (method a) was studied with microwave pulses between 100 W and 300 W at the melting point of the ligands. The 300 W pulse was chosen since it consistently produced the best yield of products. Once the reaction was cooled a solid was obtained and characterized by IR spectroscopy: the results were very similar to those of the products after recrystallization. The comparison of the IR of the melt with the IR of the crystals and that of free $SALOH_2$ (see ESI Fig. S05†) clearly shows that the organic ligands are already coordinated to the M(II) and Ln(III) ions, a fact that was supported by the formation of acetic acid during the reaction by protonation of the acetate groups from the lanthanide acetate reagent. The solid was extracted with the minimum amount of MeOH/MeCN mixture (1 : 1 in volume) and the green or pink-purple solution was left undisturbed. Crystals suitable for single crystal X-ray diffraction were obtained after 15–20 days. For complex **Co_4Gd**-MeCN, crystals of the product were obtained using only MeCN as crystallization solvent.

The complexes obtained all had the general formula $[M_4Ln(OH)_2(chp)_4(SALOH)_5(H_2O)(MeCN)(Solv)]$ (**Ni_4Gd**, **Ni_4Dy**, **Co_4La**, **Co_4Gd**, **Co_4Tb**, **Co_4Dy**). Complex **Co_4La** was always obtained in a mixture of precipitate and very small crystals. Crystals were handpicked for magnetic analysis and elemental analyses.

The alternative microwave assisted reactions with solvent (method b in Scheme 1) were tested but were only successful in some systems (Ni/Tb, Co/Dy and Co/Gd): all reactants and the solvents MeOH/MeCN (2 mL, 2 mL) were placed into the microwave reactor cavity. A 300 W microwave pulse was applied for 10 minutes at 120 °C. The lower temperature if compared to method a is mandated by the boiling point of the organic solvents. The precipitate was filtered and the solution left

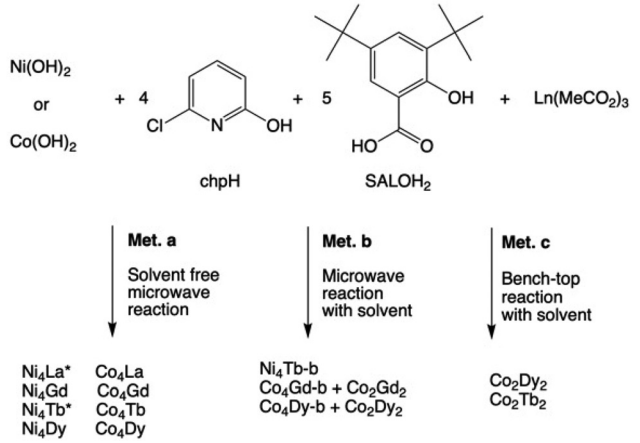

Scheme 1 Synthesis scheme showing methods a, b and c and their products. * reported in ref. 44.

undisturbed. Crystals suitable for single crystal X-ray diffraction grew in *ca.* 15 days in some systems. For the Ni/Tb system **Ni_4Tb**-b was obtained. For the other Ni/Ln systems we were not able to identify the products obtained by method b, however IR analysis of the solids obtained showed they were not the pure known Ni_4Ln species. The cobalt/Ln (Ln = Gd, Dy) reaction systems produced mixtures of products. Two types of crystals, with very similar colour and shape, appeared at similar times from the solution. The crystals were identified as complex **Co_4Gd**-b and **Co_4Dy**-b, and the new linear species $[Co_2Dy_2(chp)_2(SALOH)_8(MeOH)_4]$ and $[Co_2Gd_2(MeCO_2)(chp)(SALOH)_8(MeCN)_2]$. These by-products are also obtained for some of the Co/Ln systems from method c, doing the reaction on the bench-top, stirring at room temperature (method c in Scheme 1) for Ln = Dy, Tb but they products could not be isolated in pure form from a microwave reaction. Similar complexes have been found in the CSD with the core Co_2Ln_2 and similar organic ligands with N- or O-donors.[49–51] A complete analysis of the new Co_2Ln_2 complexes will be reported elsewhere. The species of general formula M_4Ln $[M_4Ln(OH)_2(chp)_4(SALOH)_5(H_2O)(MeCN)(Solv)]$ were only obtained from microwave assisted reactions. However, method b in the case of the Co/Gd and Co/Dy systems do not afford a pure product but a mixture of species. In fact, for the Co(II)/Ln(III) system we here observe that the microwave assisted reaction with solvent (method b in Scheme 1) affords a mixture of the products from the solvent-free microwave assisted reaction (method a in Scheme 1) and the bench-top reaction (method c in Scheme 1). To our knowledge, this Co/Ln system is unusual for microwave assisted synthesis which is often used to avoid by-products or mixtures of products.

The solvent-free microwave assisted reaction has been applied successfully to 3d–4f heterometallic coordination complexes in a carefully chosen ligand system. We believe this method can be extended to other metal–ligand systems with good results.

Description of crystal structure

Crystallographic and data collection details for **Ni_4Dy** and **Co_4La**, **Co_4Gd**, **Co_4Gd**-MeCN and **Co_4Dy** are presented in Table 1. For **Ni_4Tb**-b only the unit cell was checked and it coincided with that of Ni_4Tb.[44] Crystals were often very small and diffracted poorly due to the free-rotation of *tert*-butyl groups, thus data for complex **Co_4Gd** were collected using synchrotron radiation. Data for **Ni_4Gd** and **Co_4Tb** had low resolution so only unit cells are reported. The unit cell parameters are as expected, very similar to those of the other M_4Ln complexes and can be found in ESI Table S-C1.†

All complexes crystallize in the monoclinic space group *P*21/*c* except **Ni_4Dy**. They all have the same $M_4Ln(OH)_2$ core with small differences only in the coordinated solvent molecules. **Ni_4Dy** $[Ni_4Dy(OH)_2(chp)_4(SALOH)_5(H_2O)(MeCN)_2]$ crystallizes in the orthorhombic space group *Fdd*2. To avoid repetition, a general description of the common features of all M_4Ln complexes will be given. The asymmetric unit contains the whole molecule and disordered non-coordinated solvents, this is also true for complex **Ni4Dy**. The crystal structure and the core of **Co_4Gd**-MeCN are shown in Fig. 1.

The core consists of one Ln(III) ion linked to four M(II) ions by oxygen bridging ligands, two of these oxygens are provided by μ^3-hydroxo groups and the other four are from chp ligands. Scheme 2 shows the observed coordination modes for the chp and SALOH ligands. There are four SALOH ligands bridging

Table 1 Crystallographic parameters for the M_4Ln complexes

	Ni_4Dy	**Co_4La**	**Co_4Gd**-MeCN	**Co_4Gd**	**Co_4Dy**
System	Orthorhombic	Monoclinic	Monoclinic	Monoclinic	Monoclinic
Space group	*Fdd*2	$P2_1/c$	$P2_1/c$	$P2_1/c$	$P2_1/c$
a/Å	38.0841(17)	20.3125(12)	20.3401(13)	20.390(4)	20.3905(6)
b/Å	65.768(3)	33.4255(19)	33.317(2)	33.367(7)	33.2699(10)
c/Å	21.4176(10)	21.1033(12)	21.0558(13)	21.344(4)	21.2501(7)
α/°	90	90	90	90	90
β/°	90	115.075(3)	115.756(3)	115.83(3)	115.857(2)
γ/°	90	90	90	90	90
Volume/Å^3	53 645.1(4)	12 977.8(13)	12 851.3(15)	13 070(5)	12 972.6(7)
Z	16	4	4	4	4
Final *R* indexes $[I \geq 2\sigma(I)]$	R_1 = 0.0610	R_1 = 0.0795	R_1 = 0.0782	R_1 = 0.0784	R_1 = 0.0922
	wR_2 = 0.1817	wR_2 = 0.2124	wR_2 = 0.2497	wR_2 = 0.2475	wR_2 = 0.2805
T/K	293 K	173 K	100 K	100 K	100 K

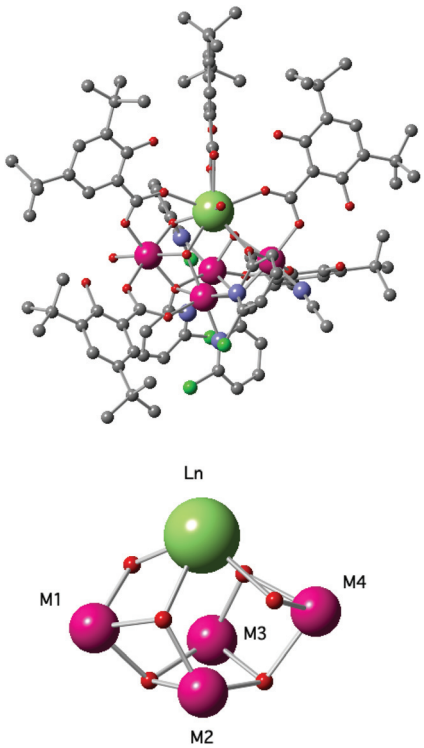

Fig. 1 Crystal structure of **Co_4Gd**-MeCN and general labelled core showing the triply bridging OH- and the bridging oxygens from chp ligands. M atoms in purple, Ln in light green, oxygen in red, nitrogen in blue, carbon in gray, chlorine in green. Hydrogen atoms have been removed for clarity.

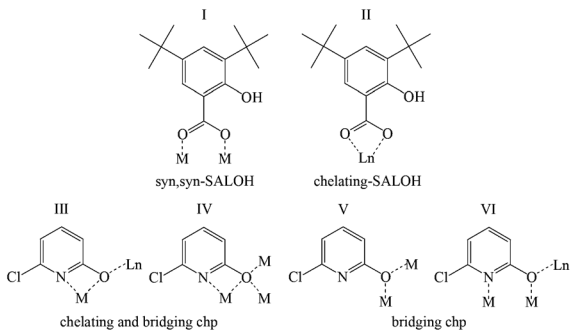

Scheme 2 Binding modes of the ligands.

every M(II) ion to the Ln(III) ion in coordination mode I. The other SALOH ligand is chelating the Ln(III) in coordination mode II. Two chp ligands are bridging three metals and chelating one metal using the oxygen and nitrogen donors in the coordination mode IV. The two remaining chp ligands are bridging the Ln(III) ion to M1 and M4 in coordination mode VI. The four M(II) ions are hexacoordinated with distorted octahedral geometries. The Ln(III) ion is ennea-coordinated with a distorted geometry. To complete its coordination sphere M1, M4 and the Ln(III) ion are bonded to terminal solvent molecules. For all the series Ln(III) is bonded to a terminal aqua ligand while the solvent molecules for M1 and M4 are either water, MeOH or MeCN. Complexes **Ni_4Gd** and **Co_4Tb** have MeOH bound to M1 and MeCN bound to M4. Complexes **Co_4Gd** and **Co_4Dy** have the same metal-OH- core as the M_4Ln series but differ in the terminal solvents: they have terminal water bonded to M1 ion. Complex **Co_4Gd**-MeCN has terminal MeCN ligands for M1 and M4.

Complex **Ni_4Dy** $[Ni_4Dy(OH)_2(chp)_4(SALOH)_5(H_2O)(MeCN)_2]$ crystallizes in the orthorhombic space group *Fdd*2 and it has two terminal MeCN bonded to the M1 and M4. Bond valence sum calculations (BVS, calculated values can be found in ESI Tables S-C2 and S-C3†)[52–54] confirm the oxidation states of the transition metal ions as M(II) and the lanthanide ion as Ln(III), as well as the oxygen atoms valence, verifying when necessary the protonation level of OH- bridging ligands, water molecules or terminal alcohol groups.

Magnetic properties

Magnetic data for crushed crystalline samples of complexes **Ni_4Gd**, **Ni_4Dy** and **Co_4La**, **Co_4Gd**, **Co_4Tb** and **Co_4Dy** were collected on a commercial SQUID. Magnetic data for complexes **Ni_4La** and **Ni_4Tb** and fitting of the susceptibility for complex **Ni_4La** were already reported in our ICF paper of 2017.[44] Magnetic susceptibility *vs.* temperature are shown as χT *vs.* T plots for the two families of complexes Ni_4Ln and Co_4Ln in Fig. 2 and 3, respectively. The data were collected in the 2–300 K temperature range at an applied field of 3000 Oe and a field of 300 Oe below 30 K. The χT product values at 300 K are collected in Table S01.† The χT product values at 300 K are in agreement with the expected values for the Ni_4Ln family: four Ni(II) ions (S = 1, g = 2.1–2.3) and one lanthanide ion, **Ni_4Dy**: Dy(III) ($^6H_{15/2}$, S = 5/2, L = 5, J = 15/2, g = 4/3) or **Ni_4Gd**: Gd(III) ($^8S_{7/2}$, S = 7/2, L = 0, g = 2.0. In the Co_4Ln family complexes the contribution of Co(II) ions is higher than the expected for a spin-only case (S = 3/2, g = 2.0) due to the presence of spin orbit coupling in hexacoordinated Co(II). For all complexes in the series the χT product values at 300 K are in agreement with four Co(II) with strong spin orbit coupling and one lanthanide(III) ion, **Co_4La**: La(III) (S = 0), **Co_4Gd**: Gd(III)

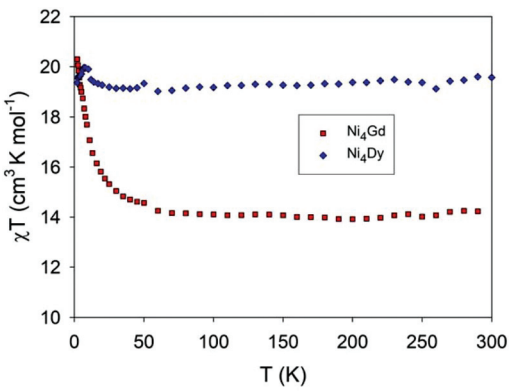

Fig. 2 Magnetic susceptibility data for Ni_4Ln complexes shown as χT *vs.* T plots. Data for complexes **Ni_4La** and **Ni_4Tb** can be found in ref. 44.

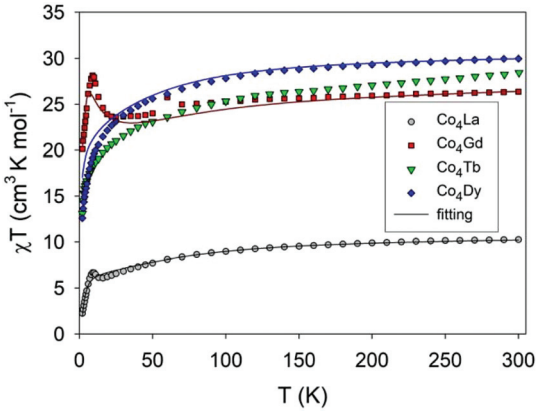

Fig. 3 Magnetic susceptibility data for Co_4Ln (right) complexes shown as χT *vs.* T plots.

($^8S_{75/2}$, $S = 7/2$, $L = 0$, $g = 2.0$), **Co_4Tb:** Tb(III) ($^7F_6$, $S = 3$, $L = 3$, $J = 6$, $g = 3/2$), **Co_4Dy:** Dy(III) ($^6H_{15/2}$, $S = 5/2$, $L = 5$, $J = 15/2$, $g = 4/3$).

The susceptibility of the M_4Ln complexes can be understood as the addition of a lanthanide ion weakly coupled to the more strongly coupled tetranuclear transition metal M_4 unit. The couplings between the transition metals in the M_4 unit are easily derived from the La derivative, for the cobalt series, that is **Co_4La**. For the Ni(II) series, the ferromagnetic coupling between the Ni(II) ions in **Ni_4La** was described in our 2017 paper as well as the ferromagnetic Ni–Tb coupling in **Ni_4Tb**, confirmed by XMCD.[44] For the Co(II) analogue there is some extent of antiferromagnetic coupling between the Co(II) centres of Co_4Ln. DFT calculations have been used to estimate the exchange coupling between Co(II) ions and between Co(II) and the lanthanide ion.

Magnetization *vs.* field data at 2 K for Ni_4Ln and Co_4Ln complexes are shown in Fig. S01.† For the family of Ni_4Ln complexes saturation is almost reached at 5 T in agreement with the ferromagnetic interactions that lead to the spin ground state. This is not the case of the Co_4Ln complexes. The fact that the magnetization value does not saturate is consistent with magnetic anisotropy associated with strong spin orbit coupling and with a combination of ferromagnetic and antiferromagnetic interactions as calculated using theoretical approaches.

Given the field-induced SMM nature of **Ni_4Tb** [44] and the large spin ground states observed and the anisotropy associated to lanthanide complexes, the dynamic magnetic properties of the new Ni_4Ln and the Co_4Ln complexes were studied. Ac magnetic susceptibility data were collected between 20 K and 1.8 K. The data showed the absence of out-of-phase signals for **Ni_4Gd** and **Ni_4Dy** with or without an applied dc field. **Ni_4Tb** is the only complex of the nickel family that shows clear field-induced SMM behaviour.[44] Clearly, the Ni_4 unit, even though it has a large spin does not have enough anisotropy to trigger SMM behaviour. The change of the transition metal from Ni(II) to Co(II) has a clear effect in the magnetic anisotropy of the complex, thus affecting the dynamic magnetic properties of the species.

All Co_4Ln complexes show peaks in the out-of-phase ac magnetic susceptibility, as expected. In a 2009 paper, Boča and Titis[55] correlated Ni(II) coordination in Ni(II) monomers with the sign of D: negative D values needed for a transition metal SMM are expected for tetragonally compressed Ni(II). Ruiz and co-workers showed for octahedral Co(II) monomers that D values are larger than for Ni(II) but sometimes positive. In polynuclear systems, an effective negative D for the molecule can be obtained by the appropriate orientation of the local ZFS tensors with respect to the molecular easy axis.[56]

Gd(III), with a large $S = 7/2$ is ferromagnetically coupled to the Co_4 unit in **Co_4Gd**, the complex has a large magnetic moment. **Co_4Gd** is an SMM and it displays an out-of-phase ac magnetic susceptibility peak at 5 K, as shown in Fig. 4 (top).

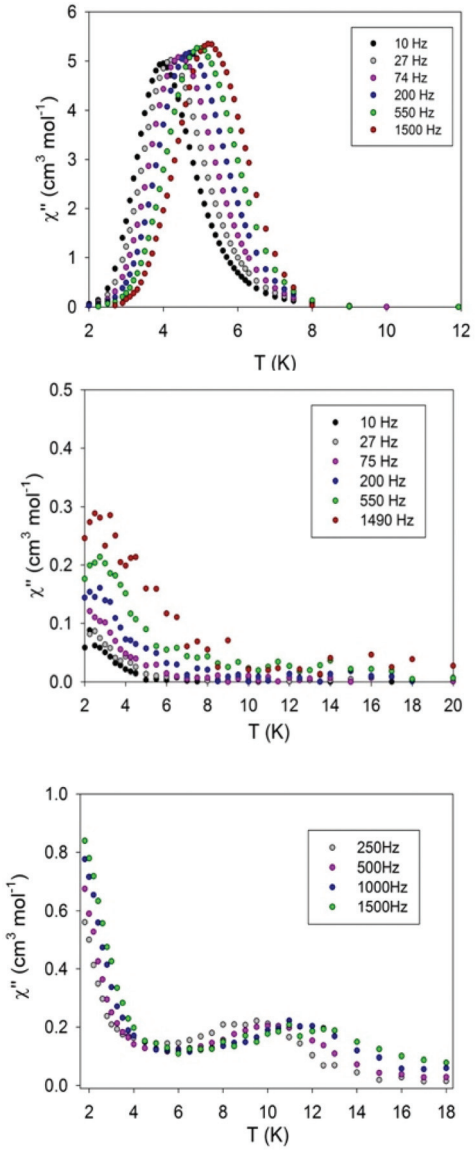

Fig. 4 Out of phase AC magnetic susceptibility plots for Co_4Gd (top), Co_4Tb with dc = 2000 G (centre) and for Co_4Dy with dc = 2000 G (bottom).

The relaxation data was fitted to Arrhenius' equation with τ_0 = 6.95×10^{-12} s^{-1} and U_{eff} = 86 K, values typical of a transition metal SMM (Fig. S03†) as good as the archetypical $Mn_{12}Ac$.[9,57] The Argand plots for **Co_4Gd** at different temperatures between 3 K and 6 K are shown in ESI Fig. S05 and 06.† The data were fitted to a Debye model for a distribution of relaxation processes with $\tau_0 = 1.06 \times 10^{-6}$–$1.53 \times 10^{-2}$ s^{-1} and α = 0.56–0.69 between 3 and 6 K. The values for each temperature can be found in the ESI Table S01.† **Co_4Tb** and **Co_4Dy** only show tails of out-of-phase ac susceptibility peaks if a dc field is applied. Thus, a static dc magnetic field was applied and ac magnetic susceptibility data were collected for **Co_4Tb** and **Co_4Dy**. The data are shown in Fig. 4 (centre) with an applied dc field of 2000 Oe. A peak appears below 6 K for **Co_4Tb** but the maximum is only observed at the highest frequencies (750 to 1500 Hz). If we compare and **Co_4Tb** to **Ni_4Tb**, the ac peak appears at higher temperatures so it is clear that using Co(II) instead of Ni(II) leads to higher energy barriers for the relaxation of the magnetization.

The ac data for **Co_4Dy** with an applied field of 2000 Oe shows two relaxation processes, one centred at 11 K and the other one below 3 K. The high-temperature process can be analysed using the Arrhenius' equation with $\tau_0 = 3.43 \times 10^{-7}$ s^{-1} and U_{eff} = 66 K (see ESI Fig. S03†). The low temperature peak is related to the application of a dc field and is important at low temperatures and low frequencies, as discussed for Ni(II), Co(II) and Cu(II) SMMs by Titis and Boca.[58,59] The ac susceptibility for **Co_4Dy** was also studied as a function of frequency at several temperatures, (ESI Fig. S04 and 05†). The data were fitted to a Debye model for a distribution of relaxation processes with $\tau_0 = 8 \times 10^{-5}$–$9.4 \times 10^{-3}$ s^{-1} and α = 0.04–0.31 between 5 and 13 K. The values for each temperature can be found in the ESI Table S01.†

Clearly the combination of a Co_4 SMM with an anisotropic lanthanide ion like Dy(III) or Tb(III) results in this case in worst properties than the combination of the Co_4 unit with Gd(III). The controversy between the importance of spin and anisotropy is clear for this family of Co_4Ln complexes: if anisotropy is good enough, increasing spin wins over increasing magnetic anisotropy in a heterometallic complex and the Co/Gd analogue **Co_4Gd** is the SMM with ac out-of-phase peaks at higher temperatures in the absence of an applied dc field, however, QTM effects are very relevant in all **Co_4Ln** complexes.

Theoretical approach to magnetic properties. For **Co_4La** the magnetic properties were modelled using a theoretical approach that shows that there is a combination of ferromagnetic and antiferromagnetic interactions between the Co(II) ions. In order to study the intramolecular exchange interactions of the **Co_4La** system, electronic structure calculations at density functional level have been performed using the Heisenberg Hamiltonian (see Computational details). The computed exchange constants as well as the involved atoms can be found in Table 2.

The overall magnetic behaviour of **Co_4La** is a combination of ferromagnetic and antiferromagnetic contributions.

The ferromagnetic interaction J_3 takes place *via* two chp ligands coordinated by both the O and N donor atoms (see Fig. 1). This interaction is responsible of the observed χT value at room temperature. The only antiferromagnetic interaction observed in **Co_4La** corresponds to J_1, and involves the μ_3-OH-bridging ligand, the O-donor atom from the chp ligand (coordination mode IV in Scheme 2) and a *syn,syn*-carboxylato group form SALOH (coordination mode I in Scheme 2). The *syn,syn*-carboxylato bridging mode is well known to favour antiferromagnetic coupling. Additional spin distributions were considered, which allows us to estimate the error on the computed exchange interactions. This statistical data validates the ferromagnetic nature of J_3 and the antiferromagnetic nature of J_1 (see ESI† material). The crystal structures of both Ni and Co complexes are very similar, however the strong spin–orbit coupling (SOC) in octahedral Co(II) results in S not being a good quantum number to describe the magnetic properties of Co(II) complexes, and one must consider J and the splitting of the m_J sublevels. Magnetostructural correlations are common for transition metals with quenched SOC like Cu(II) or Ni(II). In particular, Ni(II) cubanes with μ_3-O bridges are systems that have been particularly well studied. The complexes reported here are not cubanes, but they could be described as deformed capped cubanes, where the lanthanide caps and separates the two metal ions in one face of the cubane. The M–O–M angles in the Ni(II) series of M_4Ln are between 93° and 117° (mean Ni–O–Ni angle 102°) while for the Co(II) series are between 91° and 116° (mean Co–O–Co angle 101°). The full list of angles in the M_4Ln core can be found in ESI Table S-C4.† Magnetostructural correlations for cubanes show that the relationship between the M–O–M angle and the sign of the magnetic coupling is clear for Ni(II), with Ni–O–Ni angles below 99° leading to ferromagnetic coupling but not so straight-forward for Co(II): similar angles for Co(II) complexes lead to either ferromagnetic or antiferromagnetic coupling.[60,61] Additionally, Ni(II) dinuclear complexes bridged by phenoxo ligands display relatively large ferromagnetic coupling constants,[62] while such a magnetostructural correlation is not reported for Co(II). The theoretical approach supports the fact that an antiferromagnetic exchange pathway *via* a *syn,syn*-carboxylato bridging ligand is present in **Co_4La**.

In order to assess the Co(II)–Ln(III) coupling the magnetic data for complex **Co_4Gd**, the magnetic properties of **Co_4Gd** have also been calculated using theoretical approach. The magnetic properties of complex **Co_4Dy** have been obtained by

Table 2 Calculated exchange interactions (cm^{-1}) for complex **Co_4La**, with the corresponding bridging ligands and geometrical parameters (distances in Å and angles in degrees). Subindexes indicate metal number as shown in Fig. 1

	Atoms involved	d(Co–Co)	Bridging ligands	α(Co–O_{ox}–Co)	$J_{calc.}$
J_1	Co_1Co_2	3.119	μ_3-OH, μ_2-OR,	99.37, 92.25,	−2.67
	Co_3Co_4	3.139	μ_2-RCOO	100.14, 92.74	
J_2	Co_2Co_3	3.388	μ_2-OR	99.22, 99.06	+0.63
J_3	Co_1Co_3	3.715	μ_2-OR	117.15	+5.79
	Co_2Co_4	3.746		118.80	

rescaling by a factor 5/7 and the anisotropy of Dy(III) studied. Introducing one lanthanide ion with a magnetic moment increases the complexity of the model. DFT calculations have been performed to explore the Co(II)–Co(II) and Co(II)–Gd(III) magnetic exchange interactions in **Co_4Gd**.

To estimate four different exchange coupling constants, five spin configurations were chosen (see ESI† for details). The exchange coupling constants (Table 3) are estimated to be J_1(Co–Co) = −2.43, J_2(Co–Co) = 0.29, J_3(Co–Co) = 0.76 and J_4(Co–Gd) = 0.71 cm^{-1}. The Co–Co coupling constants (J_1 and J_2) are similar to those obtained for **Co_4La**. *Ab initio* calculation predicts that axial zero field splitting parameter of each Co is positive. The anisotropy axis of the Co(II) and Dy(III) in **Co_4Dy** are shown in Fig. 5.

The axial and rhombic zero filed splitting parameter estimated are gathered in Table 4. All four Co(II) ions are found to have local positive D value ranging from 61.0 to 94.9 cm^{-1} with significant E/D values. The variations in the magnitude of D are due to the local distortions of octahedral Co(II) with O/N donor ligands. The computed values are in accord with the values reported in the literature.[63] The values in Table 4 imply that D value increases with increasing deviation from the octahedral symmetry except Co(3) (see Table S07†). The magnitude of E/D value decreases with increasing deviation from the octahedral symmetry except for Co(2). To validate the exchange parameters obtained by DFT calculation we attempted to fit the experimental susceptibility data for **Co_4La**, **Co_4Gd** and **Co_4Dy**. The susceptibility data of **Co_4La** and **Co_4Gd** were fitted using PHI,[64] with the *ab initio* computed D and E tensors of Co(II) ions along with DFT estimated exchange coupling constants as a starting point. The best fits are shown in Fig. 3 as solid lines.

Table 3 Calculated exchange interactions (cm^{-1}) for complex **Co_4Gd**, with the corresponding bridging ligands and geometrical parameters (distances in Å and angles in degrees). Sub-indexes indicate metal number as shown in Fig. 1

	Atoms involved	d(Co–Co)	Bridging ligands	α(Co–O_{ox}–Co)	$J_{calc.}$
J_1	Co_1Co_2	3.119	μ_3-OH, μ_2-OR,	98.53, 91.95	−2.43
	Co_3Co_4	3.149	μ_2-RCOO	99.55, 93.24	
J_2	Co_2Co_3	3.149	μ_2-OR	99.55, 93.24	+0.29
J_3	Co_1Co_3	3.363	μ_2-OR	99.22, 99.06	+0.76
J_4	$GdCo_2$, $GdCo_4$	3.516, 3.487	μ^2-OR, μ_3-OH	102.04, 105.09, 102.03, 104.20	+0.71

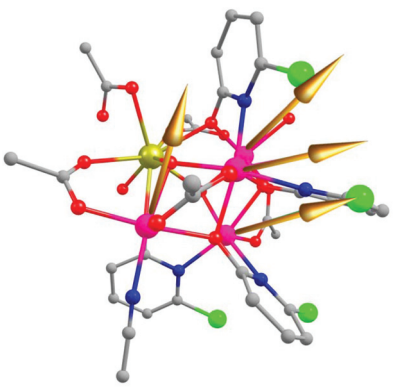

Fig. 5 The D_{ZZ} tensor the four Co(II) metal centres of complex **Co_4Dy**. Colour code: Dy-Greenish yellow, Co-Pink, Cl-Green, O-Red, N-Blue, C-Grey. Hydrogens are omitted for clarity.

Table 4 The axial and rhombic zero field parameter of Co centres

Metal centre	D (cm^{-1})	E/D
Co1	75.8	0.26
Co2	85.5	−0.03
Co3	61.0	−0.22
Co4	94.9	−0.16

For complex **Co_4La**, the J_1 and J_3 exchanges were varied to get the best fit. The best fit was obtained with the value of −0.75 cm^{-1} for J_1 and 0.85 cm^{-1} for J_3, TIP of 0.00150 cm^3 mol^{-1} and zJ' = 0.01 cm^{-1}. For complex **Co_4Gd**, the susceptibility is found to be sensitive to the exchange coupling J_1. By fixing all other parameters constant (single-ion D value of the four Co(II) centres and J_2, J_3 and J_4 interactions), good fit is obtained when J_1 = −0.90 cm^{-1}, intermolecular interaction zJ' = 0.02 cm^{-1} and TIP = 0.005 cm^{-1}. For both **Co_4La** and **Co_4Gd**, DFT computed values are overestimated compared to the values obtained from best fitting of the data. While the variation is apparent clear in J_1 for **Co_4La** and **Co_4Gd**, and in J_3 for **Co_4Gd**, since all other parameters are obtained from computational studies, this yields confidence on the estimated spin Hamiltonian parameters. The estimated Co–Ln exchange here are in line with the parameters estimated by us earlier on other [CoLn] clusters.[65,66]

Although the zero field splitting parameter of the individual Co(II) centres are positive the anisotropy axis of the individual Co(II) centres are not collinear to each other (Fig. 5). The overall magnetic behaviour is dominated by the ferromagnetic exchange (J_2, J_3 and J_4). This leads to S = 19/2 ground state for **Co_4Gd** (which is also supported by the experimental value of temperature dependent susceptibility at high temperature) leading to a large barrier for magnetisation reversal in zero field. Fig. 6 shows the population of each spin state calculated using PHI.

For complex **Co_4Dy**, simulations were performed using POLY_ANISO routine. The DFT computed exchange coupling constants (re-scaled to Dy(III)) were used for the simulation with zJ' = 0.001 cm^{-1}. This set already yields an impressive match to the experimental data highlighting the importance of parameter-free approach to the estimation of such cumbersome coupling constants.

Magnetic relaxation mechanism for the Dy(III) centre in Co_4Dy. A qualitative mechanism relaxation developed based on the *ab initio* calculations for the Dy(III) centre is shown in Fig. 7. The very large anisotropy of the Dy centre dominates over the magnetic exchange and anisotropy of the Co centres. Therefore, the overall magnetic anisotropy of the **Co_4Dy** originate from the single ion Dy(III) centre. The relaxation mecha-

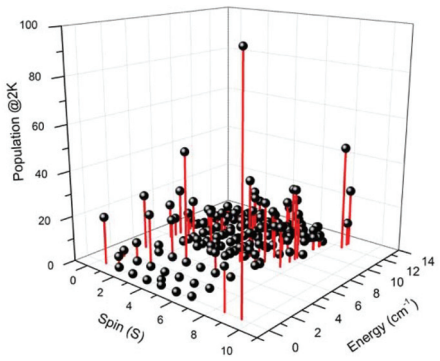

Fig. 6 Calculated population of spin states at 2 K for complex **Co_4Gd** *versus* spin state and energy; the ground state is S = 19/2.

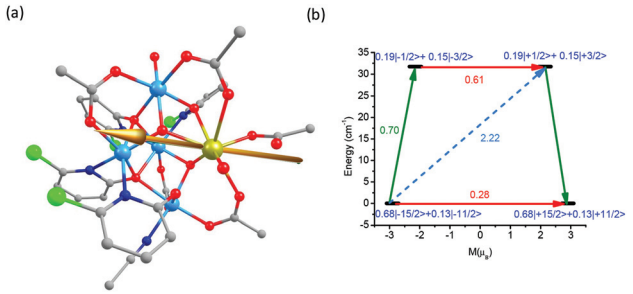

Fig. 7 (a) Modelled structure with the g_{zz} axis of the Dy centre of **Co_4Dy**. Hydrogens are omitted for clarity, colour code: Dy-Purple, Zn-Sky Blue, Cl-Green, O-Red, N-Blue, C-Grey. (b) Relaxation mechanism of Dy centre. The black line indicates the KDs as function of magnetic moments. The red line represents QTM *via* ground states and TA-QTM *via* excited states. Dashed line indicates possible Orbach process.

nism of the Dy centre implies very large QTM in the ground state and suggest no SMM characteristic (zero-field) should arise due to Dy(III) centre (Fig. 7). Continuous Shape Measure analysis around Dy(III) centre reveals that the ion resides in a trigonal-prismatic geometry (see Table S07†). The large QTM is due to the very large deviation from the trigonal-prismatic symmetry. The computed g tensors (Table S08†) reveal a large transverse anisotropy in the ground state signifying strong tunnelling and absence of SMM characteristics in zero field. The ground and first excited Kramer's doublet (KD) energy gap is estimated to be very small (31 cm^{-1}) due to the very low symmetry. The large QTM is also supported from the crystal field analysis where non-axial crystal field parameters are larger than the axial crystal field parameters (Table S10†). The probability of Orbach process ($2.22\mu_B$) is very large which reinforces it to relax *via* the first excited KD. The energy barrier for ground and first excited states is 31 cm^{-1} which is underestimated compared to the experimental blocking barrier of 46 cm^{-1}. The good agreement between the experimental susceptibility and that calculated for **Co_4Dy** using the DFT computed values re-scaled for Dy(III) highlights the importance of parameter-free approach to the estimation of such cumbersome Dy–Co coupling constants. However due to the weak nature of Co–Dy exchange, multiple low lying excited states are available, so that complex **Co_4Dy** cannot be expected to be a good zero-field SMM. The application of field might quench the tunnelling to some extent leading to the observation of SMM under applied field conditions since the probability of transition from ground to first excited KD is very large, as experimentally observed.

Experimental section

All chemicals and solvents were purchased from commercial sources and used as received. Microwave assisted reactions were performed in a CEM Discover microwave reactor. Chp stands for deprotonated 6-chloro-2-hydroxypyridine (C_5H_3ClNO). SALOH stands for monodeprotonated 3,5-ditert-butylsalicylic acid ($C_{15}H_{21}O_3$). The syntheses for complexes **Ni_4La** and **Ni_4Tb** are reported in our previous paper.[44]

$[Ni(OH)_2]\cdot xH_2O$

A solution of $NiCl_2\cdot 6H_2O$ (2.59 g, 10.88 mmol) and NaOH (0.870 g, 21.76 mmol) in 50 ml of water was stirred for 10 minutes. The green precipitate was filtered and dried for *circa* 8 hours in vacuum. Yield: quantitative. IR data (KBr, cm^{-1}): 3488 (s, b), 1645 (m), 1462 (m), 1369 (m), 655 (s, b), 416 (s); where strong (s), medium (m), weak (w), broad (b).

$[Co(OH)_2]\cdot xH_2O$

A solution of $CoCl_2\cdot 6H_2O$ (2.56 g, 10.76 mmol) and NaOH (0.860 g, 21.52 mmol) in 50 ml of water was stirred for 10 minutes. The blue-green precipitate was filtered and dried for *circa* 8 hours in vacuum. Yield: quantitative. IR data (KBr, cm^{-1}): 3629 (s), 3481 (s, b), 1652 (m), 1635 (m), 1616 (m), 1558 (m), 1506 (m), 1473 (m), 1457 (m), 850 (m, b), 668 (s, b), 501 (s, b); where strong (s), medium (m), weak (w), broad (b). XPS spectra show that the precipitate contains a small impurity of NaCl and $Co_2(OH)_3Cl$.

Method a $[Ni_4Ln(OH)_2(chp)_4(SALOH)_5(H_2O)(MeCN)(Solv)]$

(**Ni_4Gd**, Ln = Gd, Solv = MeOH; **Ni_4Dy**, Ln = Dy, Solv = MeCN): freshly prepared $Ni(OH)_2$ (100 mg, 1.088 mmol), 6-chloro-2-hydroxypyridine (140.94 mg, 1.088 mmol), Ln(III) acetate (**Ni_4Gd**, 90.95 mg; **Ni_4Dy**, 92.38 mg; 0.272 mmol) and 3,5-di-*tert*-butylsalicylic acid (338.84 mg, 1.36 mmol) were homogenized on a mortar and then placed in a microwave reactor. A 300 W microwave pulse was applied for 10 minutes at 170 °C. The resulting solid was dissolved in the minimum quantity of MeOH/MeCN (1 : 1) and then filtered warm obtaining a green solution. Green crystals grew in *circa* 20 days. **Ni_4Dy** was characterized using single crystal X-ray diffraction. For **Ni_4Gd** only the unit cell was determined.

Ni_4Gd: Yield: 92 mg (15%), based on $Gd(MeCO_2)_3$. Calculated Elemental Analysis for $C_{103}H_{131}Cl_5N_6Ni_4O_{24}Gd\cdot 0.5Gd(MeCO_2)_3$: C, 49.5%; N, 3.3%; H, 5.3%. Found Elemental Analysis: C, 49.0%; N, 3.3%; H, 5.3%. IR data (KBr, cm^{-1}): 3628 (w), 2958 (s), 2870 (m), 1653 (m), 1635 (s),

1594 (s), 1445 (s), 1392 (s), 1361 (m), 1295 (m), 1245 (m), 1202 (m), 1172 (m), 1007 (m), 943 (m), 815 (m), 795 (m), 724 (m), 668 (m); where strong (s), medium (m), weak (w), broad (b).

Ni_4Dy: Yield: 56 mg (7%), based on $Dy(MeCO_2)_3$. Calculated Elemental Analysis for $C_{110}H_{171}Cl_6DyN_8Ni_4O_{42}$: C, 45.8%; N, 3.9%; H, 5.9%. Found Elemental Analysis: C, 45.1%; N, 3.9%; H, 4.6%. IR data (KBr, cm^{-1}): 3628 (w), 2958 (s), 1653 (m), 1595 (s), 1558 (s), 1444 (s), 1361 (s), 1339 (m), 1295 (m), 1244 (m), 1165 (m), 995 (m), 933 (m), 814 (m), 793 (m), 726 (m), 699 (m); where strong (s), medium (m), weak (w), broad (b).

$[Co_4Ln(OH)_2(chp)_4(SALOH)_5(H_2O)(MeCN)(Solv)]$

(**Co_4La** Ln = La, Solv = MeOH; **Co_4Gd**, Ln = Gd, Solv = H_2O; **Co_4Gd**-MeCN, Ln = Gd, Solv = MeCN; **Co_4Tb**, Ln = Tb, Solv = MeOH; **Co_4Dy**, Ln = Dy, Solv = H_2O): freshly prepared cobalt hydroxide (100 mg, 1.088 mmol), 6-chloro-2-hydroxypyridine (140.94 mg, 1.088 mmol), Ln(III) acetate (**Co_4La**, 85.96 mg; **Co_4Gd**, 90.95 mg; **Co_4Tb**, 91.42 mg; **Co_4Dy**, 92.38 mg; 0.272 mmol) and 3,5-di-*tert*-butylsalicylic acid (338.84 mg, 1.36 mmol) were homogenized on a mortar and then placed in a microwave reactor. A 300 W microwave pulse was applied for 10 minutes at 170 °C. The resulting solid was dissolved in the minimum amount of MeOH/MeCN (1 : 1) and then filtered warm obtaining a dark pink solution. Pink crystals grew in *circa* 20 days. Complexes were characterized using single crystal X-ray diffraction. Crystals of **Co_4Gd**-MeCN were obtained extracting with only MeCN.

Co_4Gd: Yield: 188.4 mg (31%), based on $La(MeCO_2)_3$. Calculated Elemental Analysis for $C_{130}H_{173}Cl_4Co_4LaN_6O_{29}$: C, 55.7%; N, 3.0%; H, 6.2%. Found Elemental Analysis: C, 55.7%; N, 3.0%; H, 6.4%. IR data (KBr, cm^{-1}): 3274 (m, b), 2960 (s), 2904 (m), 2867 (m), 1646 (s), 1593 (s), 1558 (s), 1506 (w), 1444 (s), 1389 (m), 1360 (m), 1281 (w), 1244 (m), 1220 (w), 1201 (w), 1163 (w), 1083 (w), 988 (m), 922 (m), 890 (w), 815 (m), 793 (m), 745 (w), 722 (w), 637 (w), 529 (w); where strong (s), medium (m), weak (w), broad (b).

Co_4Gd: Yield: 44.9 mg (7%), based on $Gd(MeCO_2)_3$. Calculated Elemental Analysis for $C_{113}H_{163}Cl_7Co_4GdN_8O_{39}$: C, 46.8%; N, 3.8%; H, 5.6%. Found Elemental Analysis: C, 46.7%; N, 3.4%; H, 4.9%. IR data (KBr, cm^{-1}): 3629 (w), 3417 (m, b), 3102 (w), 2955 (m), 1982 (w), 1616 (m), 1594 (s), 1538 (m), 1442 (s), 1339 (m), 1253 (w), 1164 (m), 1068 (w), 1040 (m), 994 (m), 933 (m), 786 (m), 733 (w), 697 (m), 648 (w), 611 (m), 536 (m); where strong (s), medium (m), weak (w), broad (b).

Co_4Tb: Yield: 149.7 mg (24%), based on $Tb(MeCO_2)_3$. Calculated Elemental Analysis for $C_{98}H_{132}Cl_4Co_4N_5O_{25}Tb$: C, 50.8%; N, 3.0%; H, 5.7%. Found Elemental Analysis: C, 50.8%; N, 2.9%; H, 5.6%. IR data (KBr, cm^{-1}): 3417 (m,b), 2958 (s), 2907 (m), 2869 (m), 1652 (w), 1593 (s), 1558 (s), 1444 (s), 1391 (s), 1361 (m), 1295 (w), 1244 (s), 1202 (m), 1170 (m), 1150 (w), 1118 (w), 1007 (m), 938 (m), 814 (m), 792 (m), 745 (w), 722 (w), 643 (w), 562 (w); where strong (s), medium (m), weak (w), broad (b).

Co_4Dy: Yield: 201 mg (32%), based on $Dy(MeCO_2)_3$. Calculated Elemental Analysis for $C_{102}H_{141}Cl_5Co_4DyN_6O_{30}$: C, 48.8%; N, 3.3%; H, 5.6%. Found Elemental Analysis: C, 48.8%; N, 3.2%; H, 5.6%. IR data (KBr, cm^{-1}): 3627 (w), 3107 (w, b), 2958 (s), 2869 (w), 1652 (w), 1593 (s), 1558 (s), 1444 (s), 1392 (s), 1361 (m), 1295 (w), 1244 (m), 1202 (w), 1168 (m), 1121 (w), 1005 (w), 937 (w), 815 (w), 792 (w), 724 (w), 668 (w), 644 (w), 614 (w), 540 (w), 516 (w); where strong (s), medium (m), weak (w), broad (b).

Method b(Ni_4Tb-b, Co_4Gd-b and Co_4Dy-b)

Freshly prepared nickel or cobalt(II) hydroxide (1.088 mmol), 6-chloro-2-hydroxypyridine (140.94 mg, 1.088 mmol), Ln(III) acetate (Ln = Tb, 91.42 mg, 0.272 mmol; Ln = Gd, 90.95 mg, 0.272 mmol; Ln = Dy 92.38 mg, 0.272 mmol) and 3,5-di-*tert*-butylsalicylic acid (338.84 mg, 1.36 mmol) were homogenized on a mortar and then placed in a microwave reactor with MeOH/MeCN (2 ml/2 ml). A 300 W microwave pulse was applied for 10 minutes at 120 °C. A solution with precipitate was obtained. The precipitate was filtered and the solution left undisturbed. Crystals grew in *circa* 5 days and the products identified as **Ni_4Tb**-b, mixtures of **Co_4Dy**-b and $[Co_2Dy_2(chp)_2(SALOH)_8(MeOH)_4]$ and mixtures of **Co_4Gd**-b and $[Co_2Gd_2(MeCO_2)(chp)(SALOH)_8(MeCN)_2]$ by single crystal X-ray diffraction, IR and elemental analyses.

Characterization

X-Ray diffraction data for complexes **Ni4Dy**, **Co4Gd**-MeCN, **Co4Dy** and unit cells for **Ni4Gd**, **Ni4Tb**-b, **Co4Gd**-b, **Co4Tb**, and **Co4Dy**-b were collected on a Bruker APEXII SMART diffractometer using Molybdenum Kα microfocus (λ = 0.71073 Å) radiation source. Single crystal diffraction data for **Co4Gd** were collected at the XALOC beamline of Alba-CELLS Synchrotron (Spain) (T = 100 K, λ = 0.729 Å). Single crystal diffraction data for **Co4La** were collected at the Advanced Light Source station, at Berkeley (USA) (T = 173 K, λ = 0.71073 Å). The structures were solved by Patterson or intrinsic phasing methods (SHELXS2014 and SHELXT) and refined on F^2 (SHELXL-2014). Hydrogen atoms were included on calculated positions, riding on their carrier atoms. To calculate solvent accessible voids solvent masks were applied. CCDC 1915070 (**Ni_4Dy**), 1878755 (**Co_4Gd**-MeCN), 18335341 (**Co_4Dy**), 1878760 (**Co_4La**), 1878756 (**Co_4Gd**).† Elemental analyses (CHN) were performed at Servei de Microanàlisi in CSIC (Consell Superior d'Investigacions Científiques). Infrared spectra were collected on KBr pellets on an AVATAR 330 FT-IR at Departament de Química Inorgànica, Universitat de Barcelona. XPS experiments were performed in a PHI 5500 Multitechnique System (from Physical Electronics) with a monochromatic X-ray source (Aluminium K-alfa line of 1486.6 eV energy and 350 W), placed perpendicular to the analyzer axis and calibrated using the 3d5/2 line of Ag with a full width at half maximum (FWHM) of 0.8 eV. The analysed area was a circle of 0.8 mm diameter, and the selected resolution for the spectra was 187.85 eV of Pass Energy and 0.8 eV per step for the general spectra and 23.5 eV of Pass Energy and 0.1 eV per step for the spectra of the different elements. A low energy electron gun (less than 10 eV) was used in order to discharge the surface when necessary. All Measurements were

made in a ultra high vacuum (UHV) chamber pressure between 5×10^{-9} and 2×10^{-8} torr. Magnetic measurements were performed at the Unitat de Mesures Magnètiques of the Universitat de Barcelona on a Quantum Design SQUID MPMS-XL magnetometer equipped with a 5 T magnet. Diamagnetic corrections for the sample holder and for the sample using Pascal's constants were applied. Hysteresis measurements were performed with an array of micro-SQUIDs. This magnetometer works in the temperature range of 0.04 to 5 K and in fields up to 1.4 T with sweeping rates as high as 0.28.

Conclusions

The solvent-free microwave assisted synthesis method can be easily extended to different ligand/metal systems, in this paper we show how we can systematically change the metals in the system using this synthetic approach. The requirements are simple: ligands with low melting points that can serve as a molten reaction media on the microwave reactor. The molten ligand facilitates ion diffusion in the reaction and is key for the formation of a coordination complex. The solvent free reaction drastically reduces the use of organic solvents, being a clean method that is both cost and time efficient. In the particular case reported here, the solvent free microwave assisted synthesis has been applied to the preparation of a family of heterometallic 3d–4f M4Ln complexes, with the possibility of changing both the transition metal (M = Co(II), Ni(II)) and the lanthanide ion (Ln = La(III), Gd(III), Dy(III), Tb(III)). This produces a family of complexes with tuneable magnetic moment and magnetic anisotropy. The static and dynamic magnetic properties of the complexes reported have been studied showing that the substitution of Ni(II) for Co(II) consistently leads to better SMMs. In the Co_4Ln series, the largest magnetic moment for **Co_4Gd** as well as the lack of the spin–orbit coupling in the lanthanide ion are key for obtaining high energy barriers for the relaxation of the magnetization and to avoid relaxation by QTM. The analogues of more anisotropic lanthanide ions like Dy(III) or Tb(III) have relaxation mechanisms dominated by QTM that must be quenched in order to obtain better SMM properties.

Conflicts of interest

There are no conflicts to declare.

Acknowledgements

ECS, LRP and LC acknowledge the financial support from the Spanish Government, (Grant CTQ2015-68370-P). JC acknowledges the use of computer resources in the Consorci de Serveis Universitaris de Catalunya (CSUC). G. R. would like to thank SERB (EMR/2014/00024) for financial support. SD would like to thank to UGC for financial support in PhD.

Notes and references

1 J. Camarero, E. Coronado and A. Epstein, *J. Mater. Chem.*, 2009, **19**, 1678–1684.
2 L. Bogani and W. Wernsdorfer, *Nat. Mater.*, 2008, **7**, 179–186.
3 M. N. Leuenberger and D. Loss, *Nature*, 2001, **410**, 789–793.
4 M. Evangelisti, A. Candini, A. Ghirri, M. Affronte, E. K. Brechin and E. J. L. McInnes, *Appl. Phys. Lett.*, 2005, **87**, 072504.
5 R. Sessoli, H. L. Tsai, A. R. Schake, S. Wang, J. B. Vincent, K. Folting, D. Gatteschi, G. Christou and D. N. Hendrickson, *J. Am. Chem. Soc.*, 1993, **115**, 1804–1816.
6 R. Sessoli, D. Gatteschi, A. Caneschi and M. A. Novak, *Nature*, 1993, **365**, 141–143.
7 G. Christou, D. Gatteschi, D. N. Hendrickson and R. Sessoli, *MRS Bull.*, 2000, 66–71.
8 D. Gatteschi, *J. Alloys Compd.*, 2001, **317–318**, 8–12.
9 G. Aromí and E. K. Brechin, *Struct. Bonding*, 2006, **122**, 1–67.
10 E. K. Brechin, C. Boskovic, W. Wernsdorfer, J. Yoo, A. Yamaguchi, E. C. Sanudo, T. R. Concolino, A. L. Rheingold, H. Ishimoto, D. N. Hendrickson and G. Christou, *J. Am. Chem. Soc.*, 2002, **124**, 9710–9711.
11 E. C. Sañudo, W. Wernsdorfer, K. A. Abboud and G. Christou, *Inorg. Chem.*, 2004, **43**, 4137–4144.
12 A. J. Tasiopoulos, A. Vinslava, W. Wernsdorfer, K. A. Abboud and G. Christou, *Angew. Chem., Int. Ed.*, 2004, **43**, 2117–2121.
13 A. M. Ako, I. J. Hewitt, V. Mereacre, R. Clérac, W. Wernsdorfer, C. E. Anson and A. K. Powell, *Angew. Chem., Int. Ed.*, 2006, **45**, 4926–4929.
14 R. Sessoli and A. K. Powell, *Coord. Chem. Rev.*, 2009, **253**, 2328–2341.
15 L. Sorace, C. Benelli and D. Gatteschi, *Chem. Soc. Rev.*, 2011, **40**, 3092–3104.
16 L. Rosado Piquer and E. C. Sañudo, *Dalton Trans.*, 2015, **44**, 8771–8780.
17 S. A. Sulway, R. A. Layfield, F. Tuna, W. Wernsdorfer and R. E. P. Winpenny, *Chem. Commun.*, 2012, **48**, 1508–1510.
18 T. Pugh, F. Tuna, L. Ungur, D. Collison, E. J. L. McInnes, L. F. Chibotaru and R. A. Layfield, *Nat. Commun.*, 2015, **6**, 7492.
19 F. S. Guo, B. M. Day, Y. C. Chen, M. L. Tong, A. Mansikkamäki and R. A. Layfield, *Angew. Chem., Int. Ed.*, 2017, **56**, 11445–11449.
20 F. Guo, B. M. Day, Y. Chen, M. Tong, A. Mansikkamäki and R. A. Layfield, *Science*, 2018, **362**, 1400–1403.
21 C. A. P. Goodwin, F. Ortu, D. Reta, N. F. Chilton and D. P. Mills, *Nature*, 2017, **548**, 439–442.
22 N. Ishikawa, M. Sugita, T. Ishikawa, S.-Y. Koshihara and Y. Kaizu, *J. Am. Chem. Soc.*, 2003, **125**, 8694–8695.
23 N. Ishikawa, M. Sugita and W. Wernsdorfer, *Angew. Chem., Int. Ed.*, 2005, **44**, 2931–2935.
24 C. Wäckerlin, F. Donati, A. Singha, R. Baltic, S. Rusponi, K. Diller, F. Patthey, M. Pivetta, Y. Lan, S. Klyatskaya, M. Ruben, H. Brune and J. Dreiser, *Adv. Mater.*, 2016, 5142.

25 R. E. P. Winpenny, *Dalton Trans.*, 2002, 1–10.
26 M. Ledezma-Gairaud, L. Grangel, G. Aromí, T. Fujisawa, A. Yamaguchi, A. Sumiyama and E. C. Sañudo, *Inorg. Chem.*, 2014, **53**, 5878–5880.
27 A. Pons-Balagué, S. Piligkos, S. J. Teat, J. Sánchez Costa, M. Shiddiq, S. Hill, G. R. Castro, P. Ferrer-Escorihuela and E. C. Sañudo, *Chemistry*, 2013, **19**, 9064–9071.
28 A. Pons-Balague, N. Ioanidis, W. Wernsdorfer, A. Yamaguchi and E. C. Sanudo, *Dalton Trans.*, 2011, **40**, 11765–11769.
29 B. A. Roberts and C. R. Strauss, *Acc. Chem. Res.*, 2005, **38**, 653–661.
30 E. T. Thostenson and T.-W. Chou, *Composites, Part A*, 1999, **30**, 1055–1071.
31 A. Pons-Balagué, M. J. Heras Ojea, M. Ledezma-Gairaud, D. Reta Mañeru, S. J. Teat, J. Sánchez, G. Aromí and E. C. Sañudo, *Polyhedron*, 2013, **52**, 781–787.
32 M. Ledezma-Gairaud, L. W. Pineda, G. Aromí and E. C. Sañudo, *Polyhedron*, 2013, **64**, 45–51.
33 C. J. Milios, A. Vinslava, A. G. Whittaker, S. Parsons, W. Wernsdorfer, G. Christou, S. P. Perlepes and E. K. Brechin, *Inorg. Chem.*, 2006, **45**, 5272–5274.
34 J. Klinowski, F. A. A. Paz, P. Silva and J. Rocha, *Dalton Trans.*, 2011, **40**, 321–330.
35 J. A. Gerbec, D. Magana, A. Washington and G. F. Strouse, *J. Am. Chem. Soc.*, 2005, **127**, 15791–15800.
36 A. J. Blake, E. K. Brechin, A. Codron, R. O. Gould, C. M. Grant, S. Parsons, J. M. Rawson and R. E. P. Winpenny, *J. Chem. Soc., Chem. Commun.*, 1995, **3**, 1983.
37 E. K. Brechin, S. G. Harris, S. Parsons and R. E. P. Winpenny, *Angew. Chem., Int. Ed. Engl.*, 1997, **36**, 1967–1969.
38 E. C. Sanudo, A. A. Smith, P. V. Mason, M. Helliwell, G. Aromi and R. E. P. Winpenny, *Dalton Trans.*, 2006, 1981–1987.
39 E. C. Sañudo, C. A. Muryn, M. A. Helliwell, G. A. Timco, W. Wernsdorfer and R. E. P. Winpenny, *Chem. Commun.*, 2007, 801–803.
40 R. H. Laye, F. K. Larsen, J. Overgaard, C. A. Muryn, E. J. L. McInnes, E. Rentschler, V. Sanchez, S. J. Teat, H. U. Güdel, O. Waldmann, G. A. Timco and R. E. P. Winpenny, *Chem. Commun.*, 2005, **8**, 1125–1127.
41 E. C. Sanudo, J. Ribas and R. E. P. Winpenny, *New J. Chem.*, 2007, **31**, 1421–1423.
42 Y. Horii, K. Katoh, G. Cosquer, B. K. Breedlove and M. Yamashita, *Inorg. Chem.*, 2016, **55**, 11782–11790.
43 Y. F. Yong, J. A. Kowalski and M. A. Lipton, *J. Org. Chem.*, 1997, **62**, 1540–1542.
44 L. Rosado Piquer, E. Jiménez, Y. Lan, W. Wernsdorfer, G. Aromi and E. C. Sañudo, *Inorg. Chem. Front.*, 2017, **4**, 595–603.
45 M. Affronte, S. Carretta, G. A. Timco and R. E. P. Winpenny, *Chem. Commun.*, 2007, 1789–1797.
46 A. Ghirri, V. Corradini, V. Bellini, R. Biagi, U. del Pennino, V. De Renzi, J. C. Cezar, C. A. Muryn, G. A. Timco, R. E. P. Winpenny and M. Affronte, *ACS Nano*, 2011, **5**, 7090–7099.
47 V. Corradini, A. Ghirri, E. Garlatti, R. Biagi, V. De Renzi, U. del Pennino, V. Bellini, S. Carretta, P. Santini, G. Timco, R. E. P. Winpenny and M. Affronte, *Adv. Funct. Mater.*, 2012, **22**, 3706–3713.
48 L. Rosado Piquer and E. C. Sañudo, *Polyhedron*, 2019, **169**, 195–201.
49 Y. Zhu, A. F. Luo, B. X. Feng, A. Z. Liao, Y. Song, A. H. Huang, A. X. Tian and A. G. Sun, *Aust. J. Chem.*, 2013, **66**, 75–83.
50 S. Chen, V. Mereacre, Z. Zhao, W. Zhang and Z. He, *New J. Chem.*, 2018, **42**, 1284–1289.
51 G. Novitchi, S. Shova, Y. Lan, W. Wernsdorfer and C. Train, *Inorg. Chem.*, 2016, **55**, 12122–12125.
52 D. Brown and I. D. Altermatt, *Acta Crystallogr.*, 1985, **41**, 244–247.
53 I. D. Brown and K. K. Wu, *Acta Crystallogr., Sect. B: Struct. Crystallogr. Cryst. Chem.*, 1976, **32**, 1957–1959.
54 O. C. Gagné and F. C. Hawthorne, *Acta Crystallogr., Sect. B: Struct. Sci., Cryst. Eng. Mater.*, 2015, **71**, 562–578.
55 J. Titiš and R. Boča, *Inorg. Chem.*, 2011, **50**, 11838–11845.
56 S. Gomez-coca, E. Cremades and E. Ruiz, *J. Am. Chem. Soc.*, 2013, **135**, 7010–7018.
57 R. Bagai and G. Christou, *Chem. Soc. Rev.*, 2009, **38**, 1011–1026.
58 J. Titis, C. Rajnak, D. Valigura and R. Boca, *Dalton Trans.*, 2018, **47**, 7879–7882.
59 R. Boča, C. Rajnák, J. Titiš and D. Valigura, *Inorg. Chem.*, 2017, **56**, 1478–1482.
60 M. A. Halcrow, J. Sun, J. C. Huffman and G. Christou, *Inorg. Chem.*, 1995, **4**, 4167–4177.
61 K. Isele, F. Gigon, A. F. Williams and S. Decurtins, *Dalton Trans.*, 2007, 332–341.
62 S. Sasmal, S. Hazra, P. Kundu, S. Dutta, G. Rajaraman, E. C. Sañudo and S. Mohanta, *Inorg. Chem.*, 2011, **50**, 7257–7267.
63 S. Gómez-Coca, A. Urtizberea, E. Cremades, P. J. Alonso, A. Camón, E. Ruiz and F. Luis, *Nat. Commun.*, 2014, **5**, 1–8.
64 N. F. Chilton, R. P. Anderson, L. D. Turner, A. Soncini and K. S. Murray, *J. Comput. Chem.*, 2013, **34**, 1164–1175.
65 S. K. Gupta, A. A. Dar, T. Rajeshkumar, S. Kuppuswamy, S. K. Langley, K. S. Murray, G. Rajaraman and R. Murugavel, *Dalton Trans.*, 2015, **1**, 5961–5965.
66 K. R. Vignesh, S. K. Langley, C. J. Gartshore, B. Moubaraki, K. S. Murray and G. Rajaraman, *Inorg. Chem.*, 2017, **56**, 1932–1949.